A New Finite Element Solver using Numerical Eigen Modes for Fast Simulation of Additive Manufacturing Processes

Nachiket Patil, Deepankar Pal and Brent Stucker
Department of Industrial Engineering, University of Louisville, KY 40292

Abstract

A new efficient numerical technique has been formulated for dimensional reduction and phenomenological multi-scale simulation of additive manufacturing processes using finite element analysis. This technique is demonstrated using prismatic build volumes to represent the Selective Laser Melting powder bed fusion additive manufacturing process. The Eigen modes determined as an outcome of implementation of this technique will help to reduce the time necessary for optimization of process parameters and closed loop control. In addition to thermal simulations of the Selective Laser Melting process, this technique is also applicable to the simulation of lattice structures, layered materials such as ultrasonically consolidated laminates, thin walled coatings and development of high fidelity beam and plate theories for parts made using additive manufacturing processes. A future integration of this method with analytical Eigen wavelets will provide infinite support compared to finite support provided by directional polynomial shape functions currently used for implementation of finite element strategies. The present Eigen modes will be also useful in analysis and optimization of mask projection based additive manufacturing processes.

Introduction

Additive manufacturing has been on the forefront of innovations in engineering and has immense potential to revolutionize manufacturing. The major factors that are critical to any manufacturing technology are geometrical accuracy, mechanical properties of the produced part and process speed. These factors are important for additive manufacturing processes as well and improvement in any of these areas can lead to better optimized and reduced cost products. Process optimization based on these factors requires a good understanding of the physics and process behavior involved. The process behavior includes variation of mechanical and thermal variables across the part domain. Process behavior also depends on the part geometry and machine parameters. Simulations can help achieve real time optimization of process parameters and closed loop control. However, real time optimization requires fast simulations to be able to work at the speed of the machine. In the present work a new fast and memory efficient numerical solver for the Finite Element Method (FEM) is presented for processes involving prismatic process domains including, for instance, the full powder bed in the case of Selective Laser Melting.

Selective Laser Melting

SLM is an important additive manufacturing process in which a laser beam selectively melts a powder bed layer-by-layer to build a complex three dimensional geometry (see Figure 1). SLM has found many applications in complex aerospace parts and biomedical implants. The accuracy and microstructure of the parts manufactured in the process can be improved with better control of machine input parameters. Input parameters for SLM include beam power, scan speed, hatch pattern, recoat time and powder layer thickness. Optimization of beam power, scan speed and hatch pattern, in particular, affect the thermal behavior of the powder bed and the melt pool shape. The Melt pool shape has a significant impact on the final geometry of the built part. The thermal behavior of the full powder bed is also important from the perspective of thermal cooling rates during solidification, which determines the microstructures and phases in the final part. A detailed literature review of this area has been performed [1]. A recently developed multi-scale simulation framework known as Feed Forward Adaptive Mesh Refinement and De-refinement (FFD-AMRD) [2,3] is used in the present work for various simulations and is also used as a part of the proposed simulation framework.
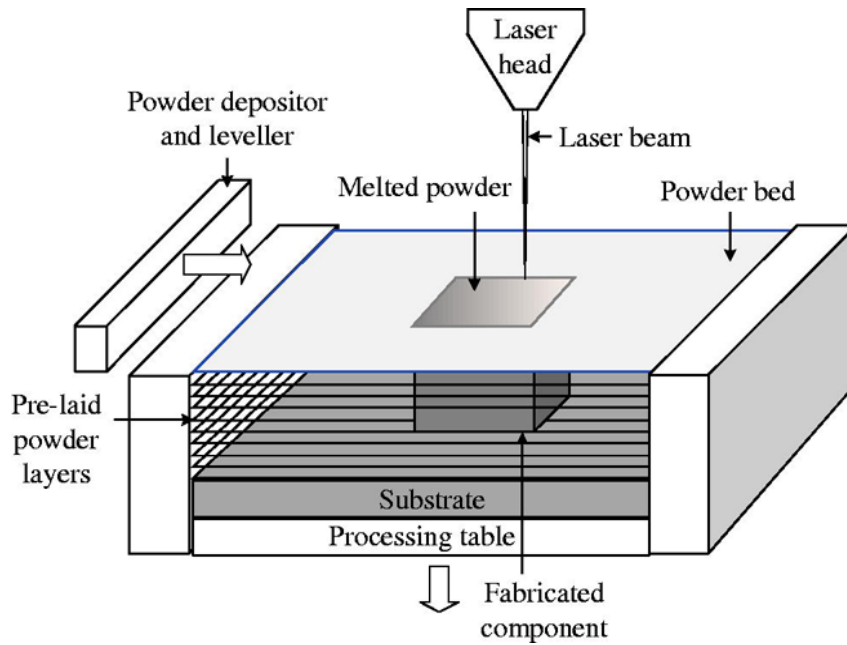
Figure 1: Schematic Diagram of the SLM process [4].

Governing equations and boundary conditions

The finite element formulation [5] for heat transfer in this work is presented in this section. Heat transfer in a material with isotropic thermal properties has the following governing equation,

$$-\left(\frac{\partial q_x}{\partial x} + \frac{\partial q_y}{\partial y} + \frac{\partial q_z}{\partial z}\right) + Q = \rho c \frac{\partial T}{\partial t}$$

(1)

where q_x, q_y, q_z are components of heat flow through a unit area. According to Fourier's law

$$q_x = -k\frac{\partial T}{\partial x}$$
$$q_y = -k\frac{\partial T}{\partial y}$$
$$q_z = -k\frac{\partial T}{\partial z}$$

(2)

where:
K = thermal conductivity coefficient of media.
Q = Q(x, y, x) inner heat generation rate per unit volume.
ρ = material density
c = heat capacity

Boundary Conditions:
Specified Temperature: $T_s = T_1(x, y, x)$ on area S_1.
Specified Heat Flow: $q_x n_x + q_y n_y + q_z n_z = -q_s$

Element Formulation:
Temperature distribution inside an element is approximated using shape functions.

$$T = [N]\{T\}$$

(3)

$$[N] = [N_1 \ N_2 \ N_3 \dots.. N_n]$$

(4)

$$T = \{T_1 \ T_2 \ T_3 \ ... \ T_8\} \tag{5}$$

Where T_i = temperature at the ith node of the element.

Temperature gradient can be written as

$$\begin{Bmatrix} \frac{\partial T}{\partial x} \\ \frac{\partial T}{\partial y} \\ \frac{\partial T}{\partial y} \end{Bmatrix} = \begin{bmatrix} \frac{\partial N_1}{\partial x} & \frac{\partial N_2}{\partial x} & ... \\ \frac{\partial N_1}{\partial y} & \frac{\partial N_2}{\partial y} & ... \\ \frac{\partial N_1}{\partial z} & \frac{\partial N_2}{\partial z} & ... \end{bmatrix} \{T\} \tag{6}$$

Global FEM Equations:
The global linear FEM equation for the transient linear problem is:

$$[C]\{\dot{T}\} + [K_c]\{T\} = \{R_Q\} \tag{7}$$

where

$$C = \int_V \rho N^T c N dV$$

$$[K_c] = \int_V B^T k B dV \tag{8}$$

$$R_Q = \int_V Q N^T dV$$

$\dot{T}$ is a nodal vector of temperature derivatives with respect to time.

Integration of Transient Thermal problem:
The Crank Nicolson integration scheme [6] or generalized trapezoidal rule is used to integrate equation (7). This rule is:

$$\{T_{n+1}\} = \{T_n\} + \Delta t \left\{(1 - \beta)\{\dot{T}_n\} + \beta\{\dot{T}_{n+1}\}\right\} \tag{9}$$

Where
$\beta = \frac{1}{2}$ is a integration parameter for the Crank Nicolson integration scheme
$\Delta t = t_{n+1} - t_n$
T_n = known nodal temperature at time t_n
T_{n+1} = temperature at time t_{n+1}

Substituting equation (7) into above equation (9) gives following equation:

$$\left(\frac{1}{\beta \Delta t}[C] + [K]\right)\{T_{n+1}\} = R_Q + [C]\left(\frac{1}{\beta \Delta t}\{T_n\} + \frac{1-\beta}{\beta}\{\dot{T}_n\}\right) \tag{10}$$

Phenomenological Multi-scale Formulation

The SLM scan pattern generally has a block pattern or continuous scan pattern where the geometry is divided into square blocks and each block is scanned subsequently with serpentine or helical patterns. A representative scan pattern is shown in figure 2.
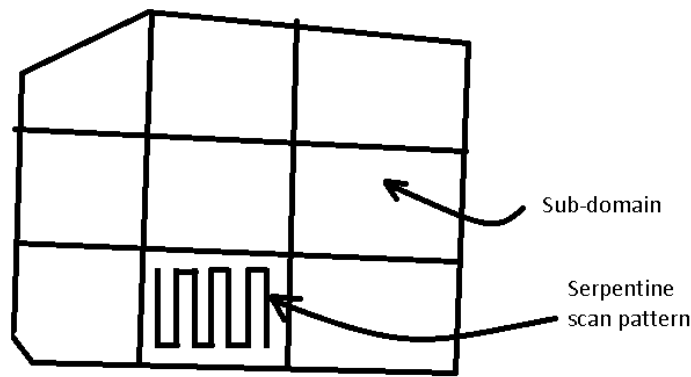
Figure 2: Scan pattern used in SLM

The temperature distributions away from the melt pool have much smaller gradients in time and space than near the melt pool. This is a multi-scale behavior where near the high gradient melt pool region, a higher mesh density is required compared to the rest of the powder bed. In the present work two separate simulations are proposed for full bed temperature variation and the sub-domain region as shown in the figure 3. These two scales are connected by specifying boundary conditions from one scale to another iteratively. The difference in sub-modeling and the proposed two scale model is that it can consider the coupling between two scales. The two scales are described separately in the following discussion.
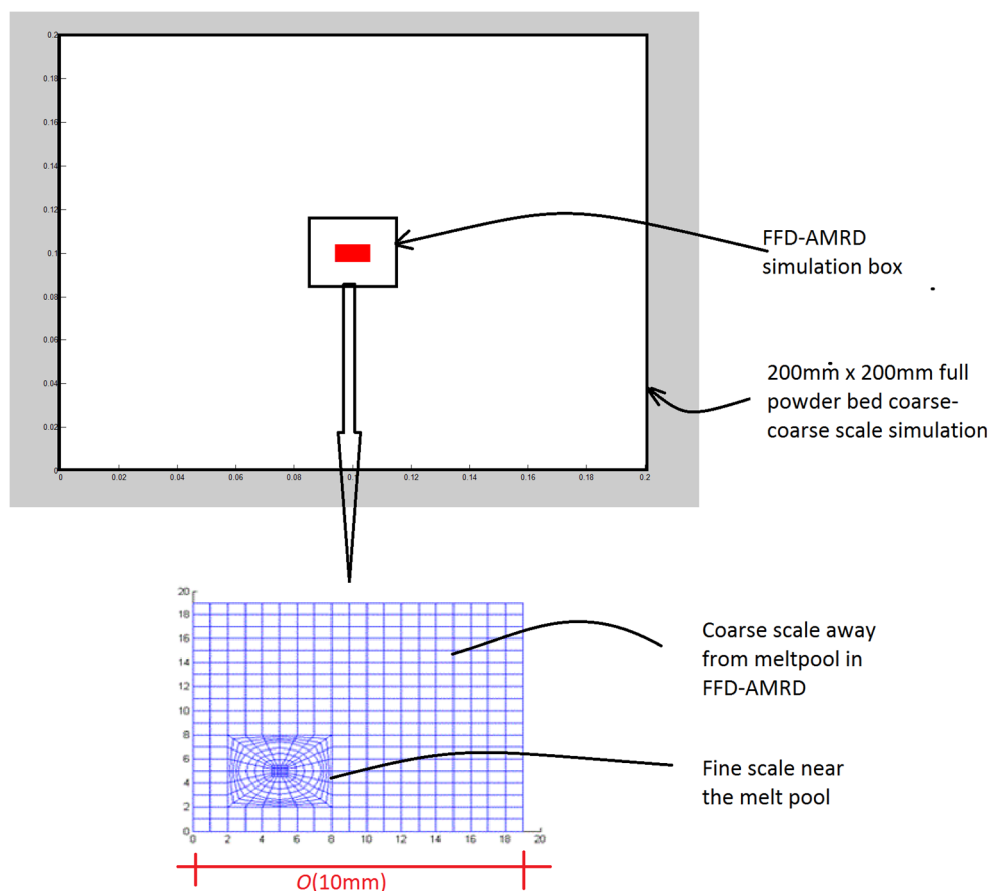

Figure 3: Multi-scale analysis framework for simulation of the SLM process

FFD-AMRD simulation covering fine-scale and fine to coarse scales:
The detailed description of the FFD-AMRD simulation software and its application to SLM were previously described in the literature [2,3]. This model covers simulation of serpentine scans in one sub-domain based on the boundary conditions provided by the coarse scale model. This model further considers various nonlinearities involved such as temperature dependent thermal material properties.

This novel numerical tool has the capability to address multi-scale interactions involved in localized spatiotemporal behaviors, for example the thermal response in case of a moving weld spot or localized deformation in sheet metal rolling processes. Traditional finite element simulations require a very fine refinement to follow the moving localized spatiotemporal response with very high spatial and temporal derivatives. This can be attributed to the fact that the scale of the localized behavior could be 10^n smaller compared to the macroscopic scale response. These two scales are efficiently bridged with FFD-AMRD software. This software has been compared to the best available commercial software and it is found to be 50 to 100 times faster and more memory efficient. The features that help this approach achieve this time and memory efficiency are intelligent element and node renumbering, efficient data transfer between different mesh domains and mesh reassembly techniques.

FFD-AMRD has the ability to model a general hatch pattern read from input files. The temperature dependent thermal properties and density data are read from input files. One of the challenges in the simulation of the SLM process had been simulation of temperature dependent material properties (for example latent heat of fusion and vaporization). In the present software these phenomena are taken care of with mathematically rigorous numerical formulations to avoid instability in time integration. The boundary conditions taken into consideration are surface convection and constant temperature boundary conditions at the base plate or on the sides, and radiation if required. The record of simulated thermal history over time leads to evolution of the solidified part geometry and phase information in the solidified part, un-melted powder that has seen a phase change, and virgin powder in its parent phase. These outputs can help when optimizing machine input parameters to achieve better cooling rates and microstructures, resulting in better part life with improved mechanical properties.

This model will be used to calculate total heat input in terms of the external flux from a laser beam and the heat absorbed by the material while changing phases, including the latent heat of vaporization and fusion.

Macro scale simulation
This simulation framework will deal with global temperature variations in the powder bed and will give temperature or flux boundary conditions to the FFD-AMRD simulation. This simulation will give the initial temperature of the subdomain and its boundary temperature as function of time. The amount of flux and its distribution as a boundary condition depends on the various energy consumptive nonlinear mechanisms involved at the fine scale behavior inside and near the melt pool.

Interaction algorithm between two scale models
The two scales are connected by the amount of heat flux transferred from the finer scale to the macroscopic scale. Flux quantification is important from the perspective of amount of heat lost or gained in the material state or phase changes. The boundary conditions and initial temperatures given to the fine scale are a function of macroscopic model thermal evolution. The coupling and information transfer between two models is shown in figure 4.
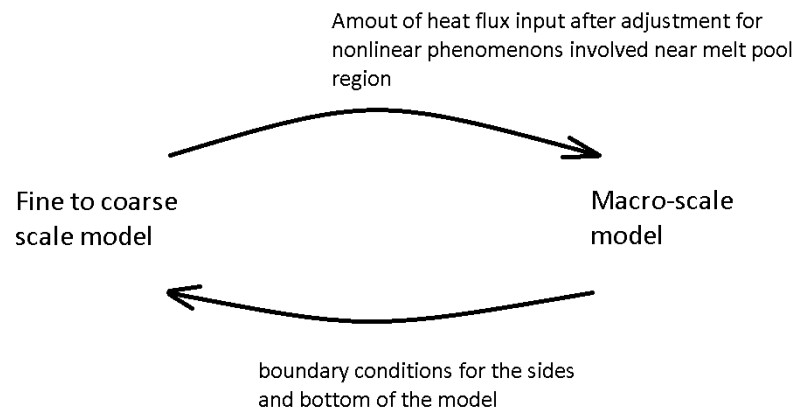

Figure 4: Interaction between two scale models

Case Study for Coupling Evaluation between Two Separate Scale Models

The coupling between two different scales is evaluated in this section with emphasis on the history dependence of the process. The history dependence is mainly due to the slowly evolving macroscopic thermal modes in the macro scale model. In the present work, only the effects of macro scale model temperatures on the fine model are evaluated. The vice versa effects of fine scale thermal effects on the macro scale model are saved for future work.

The methodology adopted for this purpose is to give different initial macro scale temperatures in FFD-AMRD simulations and find their effect on various variables of interest. The macro scale temperatures have slow variations compared to fine scale thermal behavior. This slow evolution can be exploited to simplify the analysis as well as to evaluate the coupling between two models. The assumption here is that the macroscopic thermal distribution has an almost flat distribution at the lower scale. The accuracy of such an assumption is evaluated in the next subsection. The material properties [7] of the stainless steel powder considered for this simulation are taken from literature.
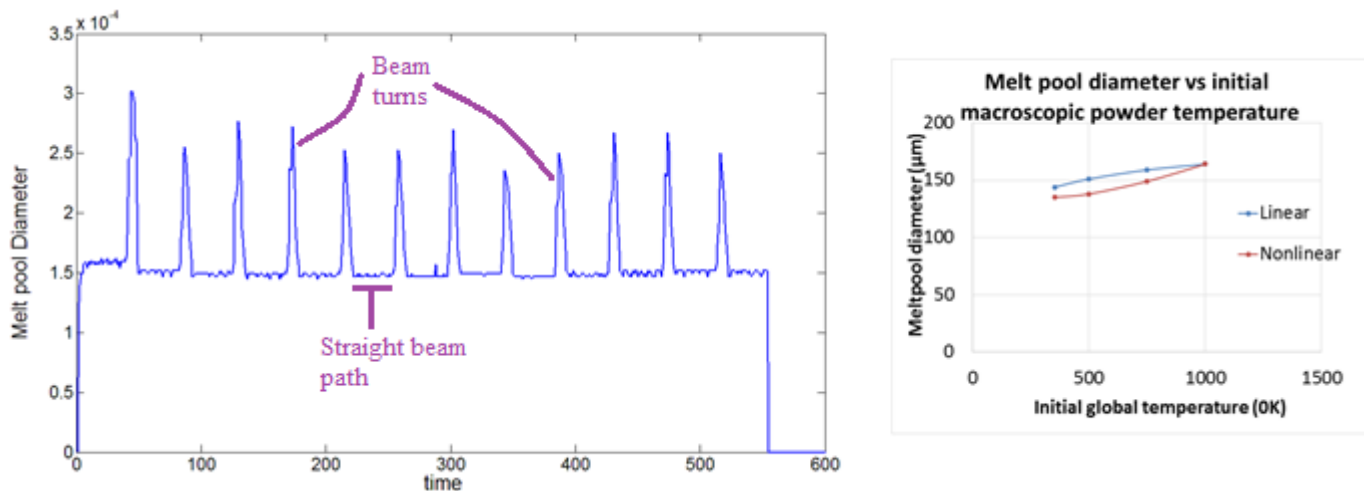
Melt pool Diameter

Figure 5: (a) Melt pool diameter variation during a subdomain hatch for the case with 750K initial temperature. (b) Effect of initial global temperature on melt pool in SLM of stainless steel powder.

Figure 5 shows the variation of the melt pool diameter in the Y direction. The melt pool diameter in the case of linear simulations is higher at lower preheating temperatures compared to the melt pool diameter in the nonlinear simulation. The reason behind the diameter increase of mere $30\mu m$ for a 647K change (from 353K to 1000K) in initial powder bed temperature for nonlinear simulation is due to the increased heat loss by heat of vaporization and fusion. These diameters are measured at the center of the scan hatch where melt pool diameters and profile are stabilized.

Cooling Rates
Two sample cooling rate plots are shown in figure 6 (a and b) for powder initial temperature of 500K and 400K. The cooling rates in both cases are not significantly different than 0.1% as it can be seen in the figure 6 (c). The effect of global heating is seen to be not very significant on the cooling rates. This leads to the conclusion that cooling rate is not a significantly coupled function of macroscopic temperature. In order to control the cooling rates, local laser characteristics such as laser power and scan speed have greater influence.

(a) 500K initial temperature

(b) 400K initial temperature
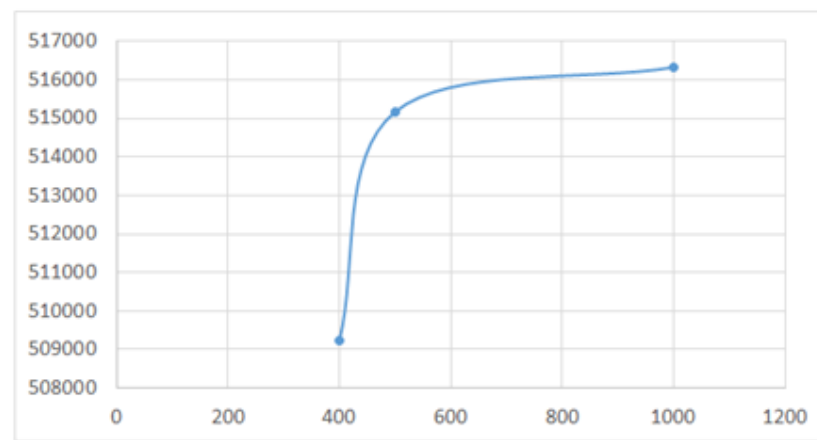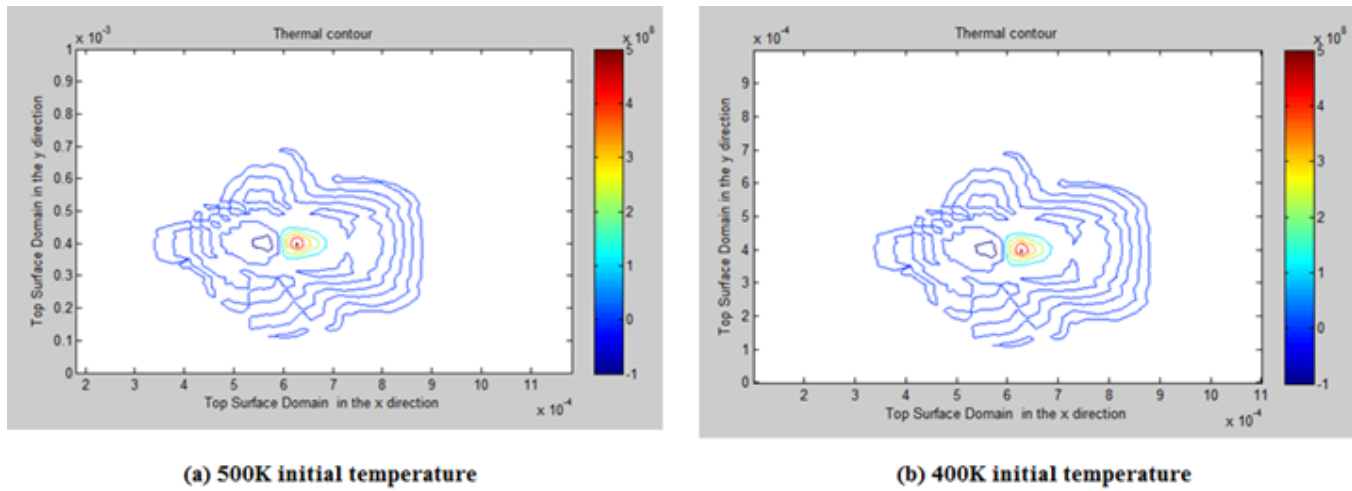
**cooling rate at a point (x=0.00062745m and y=0.00039706m)
vs initial temperature plot**

Figure 6: Cooling rates at different initial powder bed temperatures

**Cooling down for uniform
macroscopic initial temperature**

(a)

**Local temperature variations
with fast temporal scale
activated by the laser beam
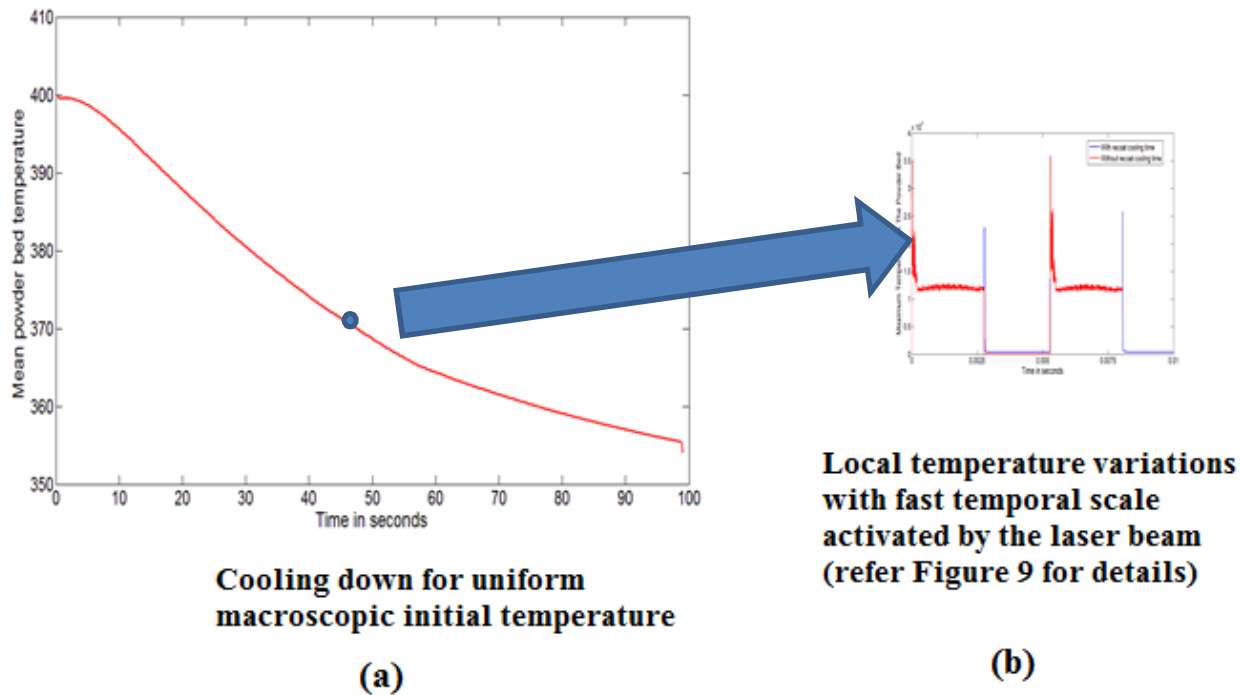(refer Figure 9 for details)**

(b)

Figure 7: Powder bed cooling down through global mode of uniform average temperature. The zoomed in picture shown the local fast temporal variation of temperature due to laser beam inside fine to coarse model.

Macroscopic powder bed cooling rates

The powder bed of size 5mm square is allowed to cool down from initial temperature of 400K. The purpose of this experiment is to compare cooling rates of the macroscopic scale compared to local thermal modes near melt pool thermal variations. Figure 7 shows a schematic concept and the actual quantitative results obtained through the numerical experiment.

The temperature variations across full powder bed are seen to be changing very slowly as shown in figure 7 (a) or have low frequencies. Whereas the local modes (figure 7 (b)) activated due to the laser beam flux have high frequency and that makes them to heat up very fast and cool down similarly at fast rate. The local modes have the major contribution towards the near Gaussian temperature distribution in the melt pool. The global modes are associated with the full powder bed temperature evolution over time.

Effect of subdomain scan pattern on thermal history

To determine the effect of scan pattern and the time required to cool down the powder around the last melt pool, a numerical experiment has been attempted. This study explores the importance of hatch pattern for successive subdomains on the thermal history. Figure 8 shows the simulated scan pattern. The subdomain on top is hatched first and then the subdomain at the bottom is hatched. The influence of first subdomain hatch is evaluate indirectly by allowing the powder bed a small time to cool down after its hatch is completed. The cool down will reduced the last melt pool spot temperatures towards the global average. This will indirectly quantify if there was any significant influence of prior neighboring subdomain scan. If significant cooling time is allowed then the effect of last melt pool spot will be almost nullified.

The maximum temperature at a particular time instance is shown in figure 9. In order to compare corresponding temperatures in two cases with respect to laser position, a plot with no cooling time is given a blank temperature offset from 0.00253 to 0.0053 second. This is to account difference in total simulation times between two cases. A cool down time of 0.0025 s is given between successive scans.

The effect of heating of the powder due to a previous nearby scan is seen to be almost negligible as the maximum and average temperature of the bed has identical variation in both cases. The bed almost cools down in a distance of 1mm to the global powder bed temperature as shown in figure 8(b). This fast cooling down of melt pool trace in prior subdomain hatch leads to negligible thermal "cross-talk" in nearby subdomain hatches. The cooling times for the melt pool is approximately 0.0005s as shown in figure 9.
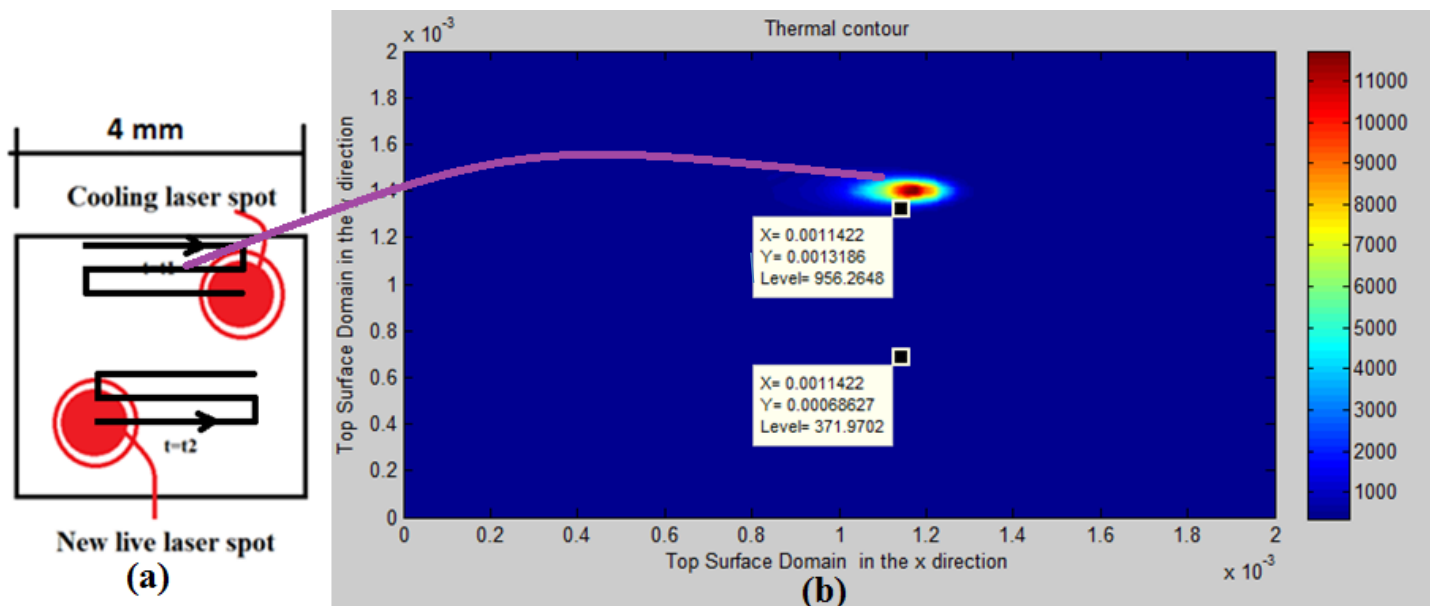

Figure 8: (a) Scan pattern used for two successive subdomains scan (b) Thermal profile at particular time in the prior subdomain scan.
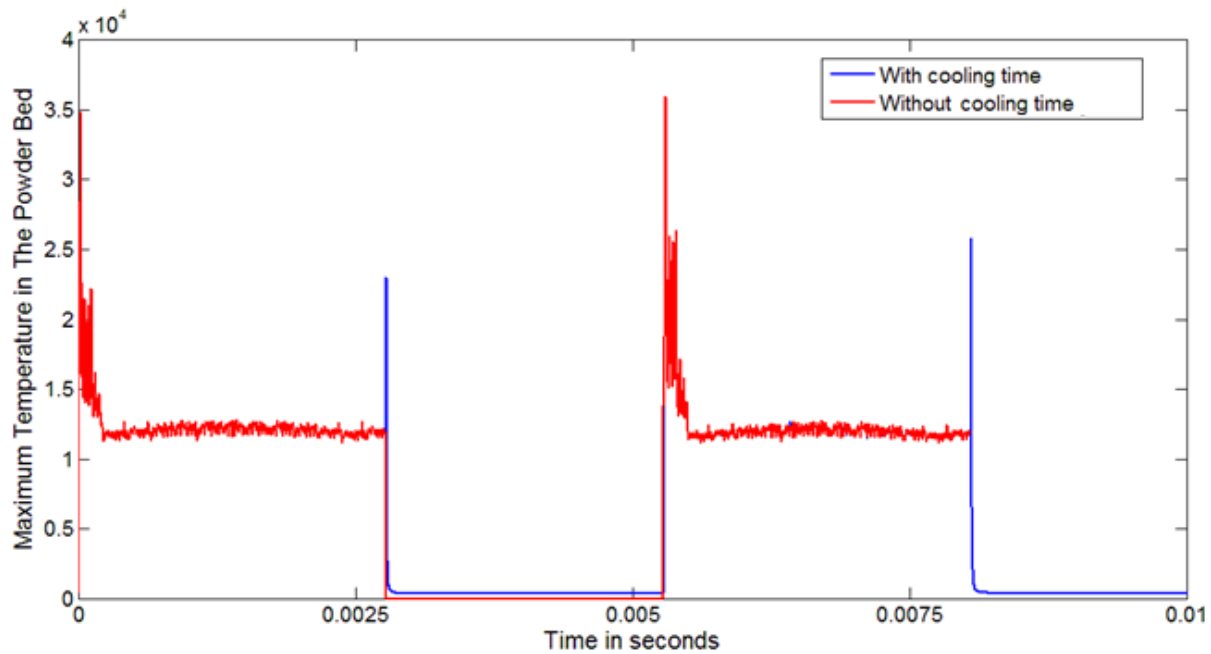
Figure 9: Maximum Temperature comparison in two cases (with and without cooling time between successive scans)

Beam Theories and Dimensional Reduction

Beam theories are developed over a long period of time, starting with the Euler Bernoulli beam theory in 1750. Over time beam theories have evolved into more and more accurate formulations. Traditional beam theories have limitations for complicated geometries, in which case ad-hoc assumptions in the beam theories lead to incorrect structural response predictions.

A recent development in beam theories is the Variational Asymptotic Method [8] (VAM) for dimensional reduction. Dimensional reduction is a term used to describe a generalized physics based beam theory used for solving partial differential equations involved in various physical phenomena. The main limitation of VAM is the energy based formulation which limits its applications in problems involving nonlinear energy dissipative phenomena like plasticity. VAM starts with an order of magnitude analysis for each term in energy expression, which is stress multiplied by strain. This helps in solving the equilibrium equation at different orders of magnitude and a solution at each order gives a particular mode of response in the dimensional reduction.

The accuracy of VAM solutions to Partial Differential Equations is limited by the fact that the order of magnitude analysis performed can be limited to a few global macroscopic modes which need not be orthogonal, particularly in the case of highly inhomogeneous cross-sections. This limitation can be attributed to the fact that in the case of in-homogeneous domains it is hard to predict variations based on superficial dimensions (order of magnitude analysis based on geometric small aspect ratio) of the prismatic structure. The local stress or strain concentrations for generalized cross-sectional geometries are hard to account for using this strategy.

Dimensional Reduction for a Prismatic Powder Bed

In the present case study a simple square cross-section with 10 times more conductive material on one side of the cross-section compared to the bulk as shown in figure 10 is considered. In order to simplify the case study a steady state problem is assumed though the mathematical formulation can be extended easily to unsteady problems.

Figure 10: Problem geometry and FEM mesh

Modal Space Derivation

The stiffness matrix for the FEM discretization described in figure 10 will have a particular pattern of sparsity. It can be described as shown below with A_i being a square matrix with a size corresponding to the number of degrees of freedom in one particular cross-section.

$$
\begin{bmatrix}
A_1 & B_1 & & & & & & \\
B_1 & A_2 & B_2 & & & & & \\
 & B_2 & A_3 & B_3 & & & & \\
 & & B_3 & A_4 & B_4 & & & \\
 & & & B_4 & A_5 & B_5 & & \\
 & & & & & \cdot & & \\
 & & & & & \cdot & & \\
 & & & & & B_{n-1} & A_n & B_n \\
 & & & & & & B_n & A_{n+1}
\end{bmatrix}
\vec{T} = \overrightarrow{Flux} =
\begin{bmatrix}
\vec{f_1} \\
\vec{f_2} \\
\vec{f_3} \\
\vec{f_4} \\
\vec{f_5} \\
\cdot \\
\cdot \\
\vec{f_n} \\
\overrightarrow{f_{n+1}}
\end{bmatrix}
\tag{11}
$$

In the case of perfectly prismatic geometry and material like a perfect beam, A_i and B_i will follow the following relation except at the free end.

$$
A_i = A
$$
$$
B_i = B
\tag{12}
$$

544

$$A_1 = A/2 \text{ (Free edge stiffness)}$$

Permutations to make the matrix upper triangle will be

$$
\begin{aligned}
P_1 &= B(A/2)^{-1} \\
P_2 &= B(A - P_1 B)^{-1} \\
P_i &= B(A - P_{i-1} B)^{-1}
\end{aligned}
\tag{13}
$$

These permutations will be operated on both sides of the equation and will create a forward wave in the right hand side and an upper triangulation on left hand side.

$$\vec{f}_{i+1} = \vec{f}_{i+1} - P_i \vec{f}_i \tag{14}$$

These equations have no closed form explicit solution or any straight forward modal space solution. This difficulty can be overcome by pre-multiplying the whole equation by B^{-1}. The permutations for the modified system of equations will look like

$$
\begin{aligned}
Pm_1 &= (B^{-1} A/2)^{-1} \\
Pm_2 &= (B^{-1} A - P_1)^{-1} \\
Pm_i &= (B^{-1} A - P_{i-1})^{-1}
\end{aligned}
\tag{15}
$$

This series of permutations have the same Eigen modes for any Pm_i. These modes are the same as of the modes of $B^{-1}A$. This is based on the property of Eigen modes that is

- The inverse of a matrix has the same Eigen Modes as that of the original matrix
- Linear equations of matrices with the same vectors have the same Eigen Vectors but different eigenvalues.

Writing Pm_i and $B^{-1}A$ in the form of modes will lead to following equations.

$$
\begin{aligned}
Pm_i &= \emptyset^T D_i \emptyset \\
B^{-1} A &= \emptyset^T K \emptyset \\
Pm_{i+1} &= \emptyset^T D_{i+1} \emptyset
\end{aligned}
\tag{16}
$$

$$\emptyset^T D_{i+1} \emptyset = (\emptyset^T K \emptyset - \emptyset^T D_i \emptyset)^{-1} \tag{16}$$

$$\emptyset^T D_{i+1} \emptyset = (\emptyset^T (K - D_i) \emptyset)^{-1} \tag{17}$$

$$D_{i+1} = (K - D_i)^{-1} \tag{18}$$

The last equation describes the evolution of Eigen values for the cross-section modes.

Converged Eigenvalues in the bulk
The Eigen values will converge asymptotically at some particular value as the permutation wave moves towards the bulk. Converged Eigen values will have the following governing equation.

$$
\begin{aligned}
D_{cov} &= (K - D_{cov})^{-1} \\
D_{cov}{}^2 - K D_{cov} + I &= [0]
\end{aligned}
$$

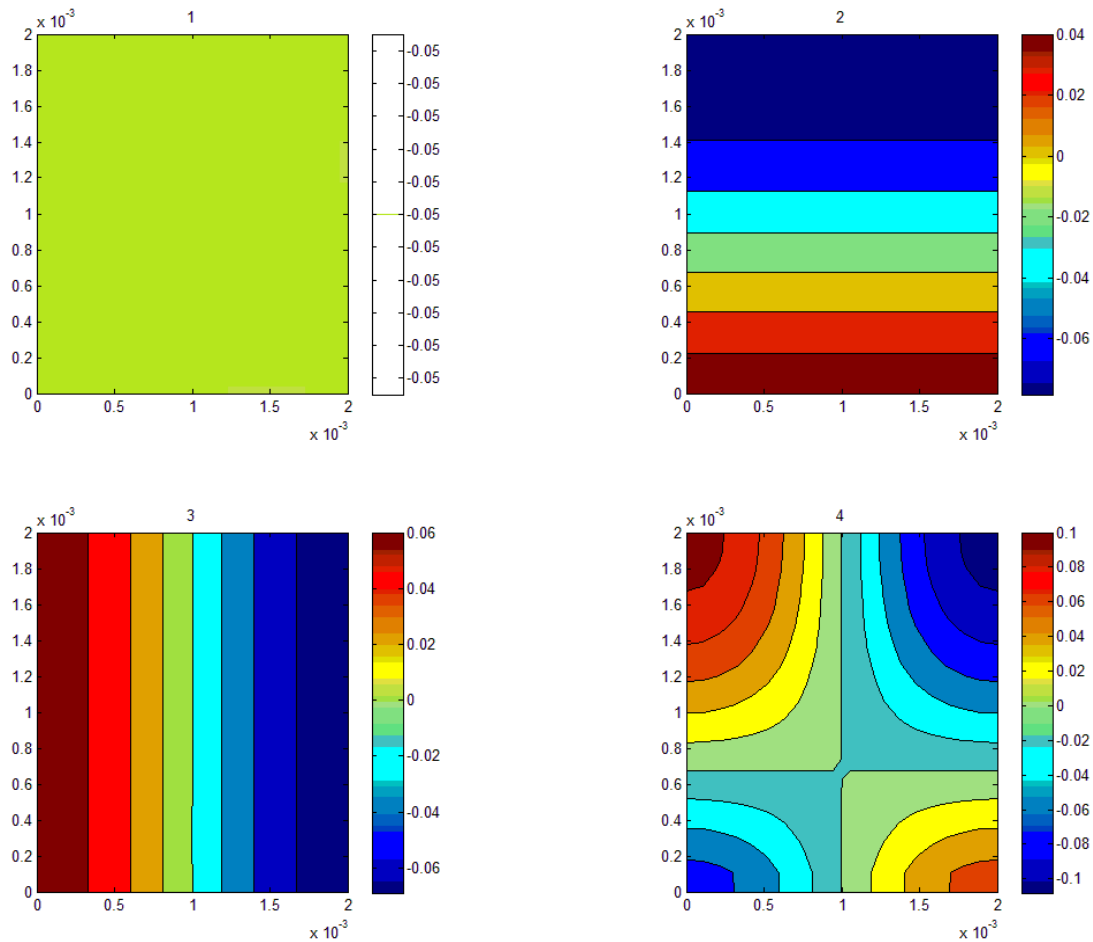This equation has an explicit solution because each matrix in it is diagonal.

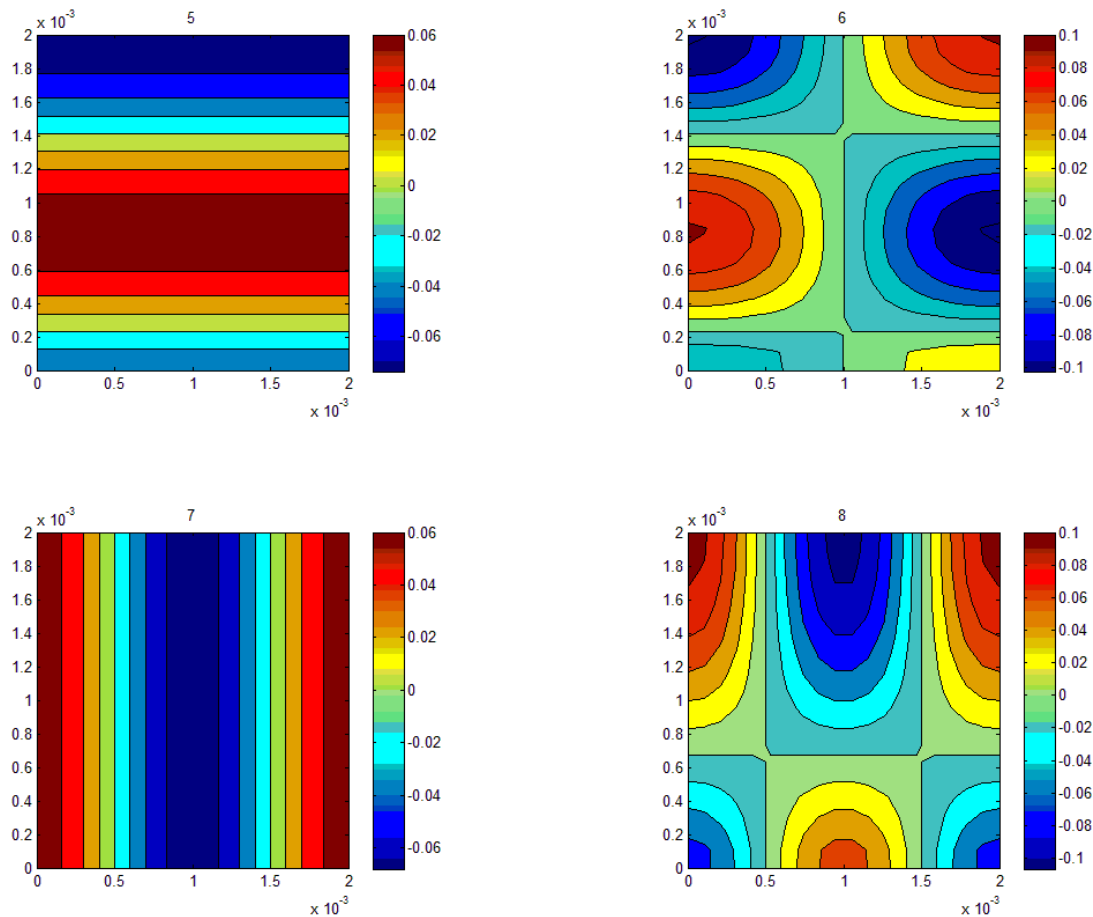Figure 11: First four significant modes for of the powder bed case study c/s

Figure 12: 5th to 8th significant modes for of the powder bed case study c/s

$$D_{cov} = \frac{\left(K \pm \sqrt{K^2 - 4}\right)}{4}$$

This proves that the minimum Eigen value for a real solution is equal to 2. This is also supported by the physics of the problem.

Eigen Modes for the prismatic powder bed: case study
The Eigen modes $\emptyset$ of the prismatic geometry shown at the start of this section are derived based on the above formulation. The first 8 significant modes are shown in figures 11 and 12. The first Eigen mode has an Eigen value equal to 1.00.

Extension of the present mathematical formulation to geometry with dissimilar layers
The assumption in the above formulation is that successive layers have material property variation across a cross-section. This assumption can be easily removed by evaluation of coupling between successive layers. Considering the number of modes that are of interest and the weak coupling between distant modes in the spectrum leads to small sized and sparse coupling matrices which need to be solved.

Conclusions

- Two separate scale models for simulation of the SLM process are proposed in order to reduce computational complexity involved in simulations.
- It is seen in the numerical experiments that the two scale model can help in developing simple laws for various parameters of interest near the melt pool region. These experiments also give a phenomenological understanding of the coupling between two scales.
- The new mathematical formulation for dimensional reduction developed in this paper has significant potential for reducing the computational complexity involved in simulations involving large number of completed build layers in the analysis.

The phenomenological understanding developed through this work is as following.
1. Cooling rates are not sensitive to the global mode preheating temperatures or initial temperatures. This also means that the cooling rates can be controlled only through laser power and velocity control.
2. The melt pool spot cool down time to near average bed temperatures is approximately found to be 0.0005s.
3. Local modes can be more efficiently influenced by energy input at the local level (which will have fast temporal scale and high frequencies). This provides an opportunity for localized preheating or post heating in order to control cooling rates or residual stresses.
4. Melt pool diameters in the case of nonlinear thermal simulation are lower compared to the diameters simulated through linear thermal simulations.

Acknowledgements

References

[1] Zeng, K., Pal, D., & Stucker, B. A review of thermal analysis methods in Laser Sintering and Selective Laser Melting, Solid Freeform Fabrication Symposium 2012, Texas Austin.

[2] Patil, N., Pal, D., Rafi, K., Zeng, K., Beeler, D., & Stucker, B., "A generalized feed forward dynamic adaptive mesh refinement and de-refinement finite element framework for spatiotemporally periodic localized

boundary conditions: Application to Metal Laser Sintering", International Journal of Thermal Sciences, xxx, xxxxxx (2013). (in communication).

[3] Pal, D., Patil, N., Rafi, K., Zeng, K., Beeler, D., & Stucker, B., "A Feed Forward Dynamic Adaptive Mesh Refinement and De-refinement (FFD-AMRD) strategy for problems with non-linear spatiotemporally periodic localized boundary conditions", J. Journal of Applied Physics, xxx, xxxxxx (2013). (in review).

[4] Mumtaz, K., & Hopkinson, N. (2010). Selective laser melting of Inconel 625 using pulse shaping. Rapid Prototyping Journal, 16(4), 248-257.

[5] Nikishkov, G.P., Programming Finite Elements in JavaTM, Springer, 2010, pp. 13-19.

[6] Crank, J. & Nicolson, P. (1947). "A practical method for numerical evaluation of solutions of partial differential equations of the heat conduction type". Proc. Camb. Phil. Soc. 43 (1): 50–67.

[7] Rafi, H., Pal, D., Patil,N., Starr, T., & Stucker, B., Microstructure and mechanical behavior of 17-4 precipitation hardenable stainless steel processed by Selective Laser Melting, (In preparation).

[8] Berdichevsky, V. L., "Variational-Asymptotic Method of Constructing a Theory of Shells," PMM , Vol. 43, No. 4, 1979, pp. 664 – 687.